The Effect of Environment on the X-Ray Emission from Early-Type Galaxies

Beth A. Brown [1] and Joel N. Bregman
Department of Astronomy, University of Michigan, Ann Arbor, MI 48109-1090
Beth.Brown@gsfc.nasa.gov, jbregman@umich.edu

ABSTRACT

In order to help understand the phenomena of X-ray emission from early-type galaxies, we obtained an optically flux-limited sample of 34 elliptical and S0 galaxies, observed with high and low angular resolution detectors on the X-ray Röntgen Satellite (*ROSAT*). Our analysis of this sample, discussed previously, suggested that the most X-ray luminous galaxies were in rich environments. Here we investigate environmental influences quantitatively and find a positive correlation between L_B/L_X and the local galaxy density. Since the local galaxy density is usually related to the density of hot intergalactic gas, we suggest that this correlation occurs because the X-ray luminosity is enhanced either through accretion of the intergalactic gas or because the ambient medium stifles galactic winds. When the ambient medium is unimportant, partial or global galactic winds can occur, reducing L_B/L_X. These effects lead to the large observed dispersion in L_X at fixed L_B. The transition from global winds to partial winds occurs in the L_B range of our sample and we argue that this transition is one of the principle reasons for the steep relationship between L_X and L_B. This is a significant departure from the steady-state cooling flow interpretation and we discuss predictions that can be tested with future observatories.

We discuss details of the data reduction not previously presented, and examine the dependence of L_X on the choice of outer source radius and background location. Effects of Malmquist bias are shown not to be important for the issues addressed. Finally, we compare the temperature deduced for these galaxies from different analyses of *ROSAT* and *ASCA* data. The *ASCA* and *ROSAT* temperatures are similar, provided that the same metallicities and Galactic absorption columns are used. However, temperatures have a dependence on the metallicity and absorption column, especially for the lower temperature systems.

---

[1]National Research Council Research Associate at NASA/Goddard Space Flight Center, Greenbelt, MD

Subject headings: galaxies: elliptical and lenticular — galaxies: ISM — X- ray: galaxies

1. Introduction

There are two primary sources for the X-ray luminosity of early-type galaxies, emission from stellar sources and optically thin radiation from a hot dilute interstellar medium (e.g., Fabbiano 1989). For the more luminous X-ray emitting ellipticals, there is little doubt that emission from hot interstellar gas is the dominant mechanism. To explain the behavior of the X-ray emission from hot gas, cooling flow models were developed, and had a number of successes. In the standard model, gas that is shed by stars is converted into hot gas with a temperature corresponding to the velocity dispersion of the stars. Radiative losses of the gas cause it to fall inward into the galaxy, releasing additional gravitational energy. This model is able to account for the observed magnitude of the X-ray luminosity, it can reproduce the X-ray surface brightness distribution, and it predicts a correlation between L_X and L_B. However, there are a few important discrepancies between theory and observation. The predicted slope of L_X–L_B relationship (approximately $L_X \propto L_B^m$, where $m = 1.6$–1.8) is not as steep as the observational relationship obtained using *Einstein Observatory* data, where $m = 1.7$–2.4. More recent work by Brown & Bregman (1998) and Irwin & Sarazin (1998) find the slope to be about 2.7, from *ROSAT* data, in clear disagreement with the steady-state cooling flow model. Another important discrepancy is the extremely large dispersion about the relationship, about two orders of magnitude in L_X at fixed L_B, first discovered in *Einstein Observatory* data (Canizares, Fabbiano, & Trinchieri 1987) and confirmed with the *ROSAT* sample (White & Davis 1997; Brown & Bregman 1998).

There have been a few explanations for the cause of the large dispersion in L_X, which is either attributed to the internal properties of the galaxy or to the external influences of the environment. D'Ercole et al. (1989) suggested that slight differences in the structure of a galaxy could lead to widely variant X-ray luminosities at fixed optical luminosity. However, this result occurs for a particular form of the supernova rate as a function of cosmic time, which may not be likely (Loewenstein & Mathews 1991). Other models that include the effects of supernova heating and galactic winds do not predict a large dispersion in L_X at the current epoch (David, Forman, & Jones 1991; Loewenstein & Mathews 1987; Vedder, Trester, & Canizares 1988).

Environmental effects are becoming more widely understood to have a significant, if

not central influence on the X-ray properties of a galaxy. One effect is stripping of gas from a galaxy as it passes through the ambient cluster medium (Takeda, Nulsen, & Fabian 1984; Gaetz, Salpeter, & Shaviv 1987). This is likely to be important in the richer clusters, but most current samples do not contain very rich clusters (the Virgo Cluster being the richest). Although there is evidence for stripping for NGC 4406 in Virgo, early-type galaxies in Virgo are not X-ray underluminous in general, so stripping is probably the exception rather than the rule. Another environmental effect is accretion of material onto galaxies, which can raise the X-ray luminosity substantially (Brighenti & Mathews 1998) and probably is most important in gas-rich group and cluster environments. A third environmental effect is the ability of an ambient medium to stifle a galactic wind, causing those galaxies to retain their gas and become more X-ray luminous than field galaxies (Brown & Bregman 1998).

In Brown & Bregman (1998), we presented the X-ray luminosities of a complete optically-selected sample of 34 early-type galaxies in the 0.5–2.0 keV *ROSAT* band. We noticed that the galaxies with the largest values of L_X (for a given L_B) were in the more populated regions (the Virgo or Fornax clusters, or in the centers of groups) of the sample, suggesting that being in moderately rich environments enhances the X-ray emission of a system. This trend may differ from that reported by White & Sarazin (1991), who found that lower-X-ray luminous galaxies had 50% more bright neighboring galaxies than higher-X-ray luminous galaxies. To further assess the importance of environment upon X-ray luminosities, we advance our previous work by analyzing the X-ray properties of our sample in the context of a quantitative measure of the galactic richness provided by Tully (1988). In addition, we present information on data processing, sample bias, temperature distribution, and several other issues not discussed in our previous Letter.

2. Galaxy Sample and Data Processing

The criteria for including a galaxy in this work is established in Brown & Bregman (1998). The targets (see Table 1) are detected at the $\geq 97\%$ confidence level, and include twelve galaxies lying within the poor clusters of Fornax and Virgo, with the remainder either isolated or lying in loose groups. For the purpose of this survey, we used PSPC data in the processing rather than HRI data when available, since HRI data contains no spectral information (Table 2).

Data analysis was performed using the PROS system under NOAO's IRAF (software written specifically for X-ray data) with an objective of obtaining a well-defined L_X for each galaxy in the sample (§2.1), and T_X (X-ray gas temperature) when possible. Spatial analyses (§2.2) were performed on images using a blocking factor of eight for the normalized

Table 1: Optical Galaxy Properties

Name	Type	l	b	B_T^0	log σ	D	r_e	logL_B	ρ
		(deg)		(mag)	(km/s)	(km/s)	($''$)	(ergs/s)	Mpc^{-3}
N 0720	E	173.02	-70.36	11.16	2.392	2050 ±435	38.58	43.65 ±0.06	0.25
N 1316[a]	S0	240.16	-56.69	9.40	2.401	1422 ± 88	80.14	44.04 ±0.06	1.15
N 1344	E	229.07	-55.68	11.11	2.204	1422 ± 88	38.38	43.35 ±0.06	0.28
N 1395	E	216.21	-52.12	10.94	2.412	1990 ±187	45.07	43.71 ±0.06	0.55
N 1399	E	236.72	-53.63	10.55	2.491	1422 ± 88	42.37	43.58 ±0.06	1.59
N 1404	E	236.95	-53.56	10.89	2.353	1422 ± 88	26.72	43.44 ±0.06	1.59
N 1407	E	209.64	-50.38	10.57	2.455	1990 ±187	71.96	43.86 ±0.12	0.42
N 1549	E	265.41	-43.80	10.58	2.312	1213 ±256	47.44	43.43 ±0.06	0.97
N 2768	E	155.49	40.56	10.93	2.296	1532 ±325	49.44	43.49 ±0.12	0.31
N 3115	S0	247.78	36.78	9.95	2.425	1021 ±215	32.32	43.53 ±0.06	0.08
N 3377	E	231.18	58.31	11.13	2.116	857 ±126	32.75	42.91 ±0.12	0.49
N 3379	E	233.49	57.63	10.43	2.303	857 ±126	35.19	43.19 ±0.06	0.52
N 3557	E	281.58	21.09	11.13	2.465	2399 ±509	37.10	43.80 ±0.06	0.28
N 3585	E	277.25	31.17	10.53	2.343	1177 ±249	38.04	43.42 ±0.06	0.12
N 3607	S0	230.59	66.42	10.53	2.394	1991 ±242	65.49	43.88 ±0.12	0.34
N 3923	E	287.28	32.22	10.52	2.335	1583 ±236	52.16	43.68 ±0.06	0.40
N 4125	E	130.19	51.34	10.58	2.359	1986 ±295	58.39	43.86 ±0.12	0.34
N 4278	E	193.78	82.77	11.02	2.425	1470 ±218	32.89	43.42 ±0.06	1.25
N 4365	E	283.80	69.18	10.64	2.394	1333 ± 71	56.57	43.48 ±0.06	2.93
N 4374	E	278.20	74.48	10.13	2.458	1333 ± 71	54.47	43.69 ±0.06	3.99
N 4406	E	279.08	74.64	9.87	2.398	1333 ± 71	89.65	43.79 ±0.06	1.41
N 4472	E	286.92	70.19	9.32	2.458	1333 ± 71	103.61	44.01 ±0.06	3.31
N 4494	E	228.62	85.32	10.69	2.095	695 ±147	45.13	42.90 ±0.06	1.04
N 4552	E	287.93	74.97	10.84	2.417	1333 ± 71	30.00	43.40 ±0.06	2.97
N 4621	E	294.37	74.36	10.65	2.381	1333 ± 71	45.54	43.48 ±0.12	2.60
N 4636	E	297.75	65.47	10.20	2.281	1333 ± 71	101.14	43.66 ±0.06	1.33
N 4649	E	295.87	74.32	9.77	2.533	1333 ± 71	73.42	43.83 ±0.06	3.49
N 4697	E	301.63	57.06	10.03	2.218	794 ±168	73.51	43.28 ±0.06	0.60
N 5061	E	310.25	35.66	11.06	2.282	1196 ±253	25.51	43.22 ±0.06	0.31
N 5102	S0	309.73	25.84	10.57	1.820	155 ± 15[b]	23.29	41.64 ±0.12	0.17
N 5322	E	110.28	55.49	11.09	2.350	1661 ±352	34.76	43.50 ±0.12	0.43
N 5846	E	0.43	48.80	10.67	2.444	2336 ±284	82.61	43.96 ±0.12	0.84
I 1459	E	4.66	-64.11	10.88	2.488	2225 ±472	34.03[c]	43.83 ±0.06	0.28
N 7507	E	23.44	-68.04	11.15	2.377	1750 ±371	31.41	43.52 ±0.06	0.09

Hubble galaxy type (col 2) and local galaxy densities (column 10) from Tully (1988). Galactic coordinates (cols 3-4) from NED. Total B_T^0 magnitudes, velocity dispersions, and distances (cols 5-7) from Faber et al. (1989). Effective radii and blue optical luminosities (cols 8-9) derived from Faber et al. (1989) values.

[a]Velocity dispersion from Roberts et al. (1991) adopted. Fornax cluster distance adopted for galaxy distance.

[b]Distance for NGC 5102 from McMillan et al. (1994).

[c]The effective radius, r_e, for IC 1459 adopted from RC3 catalog.

Table 2: Galaxy Observations

Name	Detector	Sequence no.	Livetime (sec)	Photon Counts total no. in $4r_e$	ΔCounts
N 0720	PSPC	rp600005n00	22169	1698.5	55.2
N 1316	PSPC	rp700437n00	23067	3277.2	92.1
N 1344[a]	PSPC	rp600529	4947	25.4	9.2
N 1395	PSPC	rp600133n00	19754	1373.4	53.2
N 1399	PSPC	rp600043n00	52009	18009.2	186.4
N 1404	PSPC	rp600043n00	52009	13408.9	131.6
N 1407	PSPC	rp600163n00	20971	2388.8	71.0
N 1549	PSPC	wp600623n00	15320	477.1	34.8
N 2768	PSPC	rp60052700	4771	136.5	18.6
N 3115	PSPC	rp600120n00	7452	121.9	18.0
N 3377[a]	HRI	rh600830n00	33876	87.4	25.5
N 3379	HRI	rh600829n00	24240	169.7	67.6
N 3557	PSPC	wp600464a01	19628	261.4	29.7
N 3585	PSPC	rp60052400	5199	49.5	11.8
N 3607	PSPC	rp600263n00	23865	1267.1	63.4
N 3923	PSPC	rp600533n00	22377	1456.1	49.7
N 4125	PSPC	rp600253n00	5709	434.3	30.3
N 4278	PSPC	rp701413n00	3413	170.8	17.3
N 4365	PSPC	rp600009n00	4213	632.4	47.6
N 4374	HRI	rh600493n00	26237	1609.9	89.1
N 4406	PSPC	wp600105	22141	19590.6	203.5
N 4472	PSPC	rp600248n00	25971	21015.7	191.7
N 4494	PSPC	rp600162n00	11638	98.6	39.0
N 4552	PSPC	wp600586n00	16671	1811.2	51.0
N 4621	PSPC	rp600017n00	13096	164.7	34.1
N 4636	PSPC	rp600016n00	12100	10943.4	139.2
N 4649	PSPC	rp600017n00	13096	5423.8	93.7
N 4697	PSPC	rp600262a02	45259	2361.7	98.8
N 5061[a]	PSPC	rp600528	6516	28.6	8.9
N 5102[a]	PSPC	rp60052600	8937	36.7	11.7
N 5322	PSPC	rp600270n00	31556	502.6	43.4
N 5846	PSPC	rp600257	8808	3653.3	77.7
I 1459	PSPC	rp600266n00	32707	2605.4	59.6
N 7507[a]	HRI	rh600684n00	5469	22.4	12.0

[a]Total photon count tabulated within $1r_e$ and extrapolated to $4r_e$.

PSPC data (neglecting the softest energy channels, PI < 20), creating 4 arcsec pixels. Blocking factors of two or four were used for HRI data resulting in 1-2 arcsec pixels. Spectral analyses (§2.3) were performed on normalized QPOE files using the same regions chosen for the spatial analyses, and binned according to the quality of the data.

2.1. Source and Background

The extent of the region within which the X-ray flux is determined (the source), and the image regions chosen for background subtraction, can have a significant effect on the determination of L_X because the galaxies in our sample may sit in clusters or loose groups. Brown & Bregman (1998) briefly state the source and background radial limits, and justifies the use of de Vaucouleur's half-light radius, r_e, as the basis for those limits. We chose to use a $4r_e$ radius for the advantages it offers. A circle of $4r_e$ is large enough to be resolved by the *ROSAT* PSPC for each galaxy, yet small enough to avoid possible cluster emission problems. For our five weakest targets (NGC 1344, NGC 3377, NGC 5061, NGC 5102, and NGC 7507) background emission dominates the signal when going out to $4r_e$. We therefore obtained the flux within $1r_e$, to get its best measure while maximizing the S/N. That value is then multiplied by a factor of 1.58 to extrapolate the flux out to $4r_e$. The correction factor is obtained by taking the ratio of a beta model (β=0.5, $r_{core} = r_e/11$) integrated from 0 to $4r_e$ to one integrated from 0 to $1r_e$.

The background is chosen based on our desire to examine L_X only within $4r_e$. If the background is defined to be a region far from the source center, as is usually done, there may still exist cluster emission past $4r_e$ surrounding the source. To establish a flux within $4r_e$, the excess emission along our line of sight must be removed. The best way to accomplish this is to subtract an annulus within which the mean surface brightness equals the mean surface brightness of unwanted emission in front of and behind the source. We mathematically determined the radial boundaries of this annulus, using a beta model for extended emission in elliptical galaxies of the form

$$I_X = I_o[1 + (r/r_{core,X})^2]^{-3\beta+0.5} \quad (1)$$

where I_o is the central surface brightness, and $r_{core,X}$ is the core radius of the X-ray emission. Although an infinite range of inner and outer radii is possible, we find that, to maximize the signal-to-noise, a unique solution of $r_1 = 4r_e$ and $r_2 = 6.3r_e$ exist for $\beta = 0.5$.

2.1.1. NGC 4494

One galaxy in the sample, NGC 4494, lies far off-axis ($\sim 45'$ off). At this radius, the PSF becomes large and distorted, so we needed to correct for the difference between the on-center position and its off-axis position. We could not simply scale the amount within $1r_e$ to $4r_e$ because $1r_e$ is significantly smaller than the PSF of the instrument, so the instrument scatters most of the photons out of $1r_e$. This is the only object that we have where that is true. Instead, we chose a circle of radius $240''$ as the source, and similar sized circles on either side as the background. As a comparison, we calculated the flux using an annular background 4–6.3 r_e from the center of the source which resulted in only a 10% difference, smaller than the uncertainty due to photon statistics.

2.2. Spatial Analysis

Spatial analysis was performed on the data in order to compare our well defined choice of background with backgrounds taken at large radii. We first determined the total photon count (proportional to the flux) in a $4r_e$ circle using the 4–6.3 r_e background (see Table 2). This flux was then compared to one obtained by subtracting a background region beyond the extent of the X-ray emission. This background region was also taken to be an annulus, and was typically located at $> 7r_e$ from the galaxy center. The comparisons show that only for 36% of the galaxies is there a difference greater than 10% between taking a background as detailed above, and a more traditional background (neglecting the five weak detections and NGC 4494). We find that differences greater than 10% only exist for four of the galaxies (NGC 1395, NGC 1399, NGC 4406, and NGC 4472) when photon count errors are taken into account, and 68% of the galaxies show differences of less than 5% (Figure 1).

2.3. Spectral Analysis

We used a Raymond-Smith plasma model for spectral fits, succinctly discussed in Brown & Bregman (1998). Abundances were held at 0.5 solar since the reliability with which they can be determined from the *ROSAT* PSPC has been questioned (Bauer & Bregman 1996). A recent paper by Loewenstein & Mushotzky (1997) indicate that the metallicity for the galaxies that they observed with ASCA is about 0.5 solar, with scatter, making our choice a reasonable one. Single-temperature models were preferred over two-temperature models when acceptable χ^2_ν values could be obtained ($\chi^2_\nu > 1.46$ for 30 degrees of freedom). For NGC 4472, an acceptable fit could not be obtained with either a single-temperature

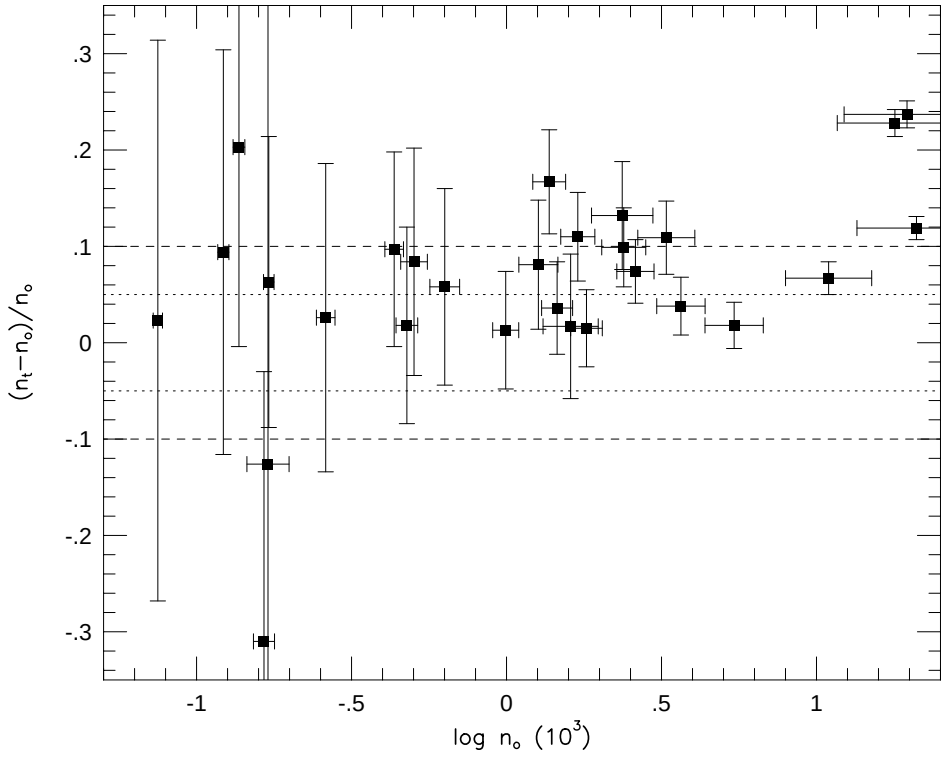

Fig. 1.— The percent difference in the number of background-subtracted photon counts within a radius of $4r_e$ using a background at 4-6.3r_e (n_o) and a background taken at large radii (n_t) against log n_o. The dotted and dashed lines are at 5% and 10% respectively.

or two-temperature model with 50% abundances, so a single-temperature model with 0.8 solar abundance was used. For NGC 1399 and NGC 1404, we also allowed the Galactic N_H column density to be a free parameter within a limited range ($20.1 \leq \log N_H \leq 20.5$ and $20.1 \leq \log N_H \leq 20.3$, respectively in cm^{-2}) to obtain an acceptable fit.

Temperatures cannot be accurately fitted for low-count (i.e., < 300 counts) PSPC objects, or HRI galaxies (no spectral information). However, a fit must be performed to the data to obtain a flux using PROS software. Therefore, the data for these few galaxies were rebinned into single bins, and fitted for the normalization only. We assumed a fixed $T_X = 3/2T_\sigma$ (typical of the findings of Davis & White 1996) except for NGC 5102 and NGC 4494 where we used temperatures of 0.5 keV and 0.3 keV respectively, since the lower calculated temperatures led to clearly unacceptable fits. The stellar velocity dispersion temperature, T_σ, is calculated according to

$$kT = \mu m_p \sigma^2, \tag{2}$$

where μ is the mean molecular weight, and σ is the one-dimensional stellar velocity dispersion.

After fitting the data, fluxes were obtained for two energy ranges – 0.5–2.0 keV and 0.1–2.0 keV – using the intrinsic spectrum found for each source, and fitted temperatures when available. Luminosities were then calculated using distances derived from Faber et al. (1989) and an $H_0 = 50$ km/s/Mpc, with the exception of NGC 5102 for which no distance was given in the Faber et al. (1989) catalog (the McMillan, Ciardullo, & Jacoby 1994 distance is used for NGC 5102). In the past, using these distances has significantly reduced the dispersion about L_X–L_B line by increasing the internal consistency of distances (Donnelly, Faber, & O'Connell 1990). Errors in the luminosity, due to uncertainties in the Galactic N_H column density (typically 5–10%) and uncertainties in photon counts, were examined and calculated. In all cases, errors in the photon statistics were found to be significantly greater than errors introduced from the uncertainty in the Galactic N_H column.

3. Analysis of the Observational Results

We have reported briefly our findings of L_X and T_X for this study in Brown & Bregman (1998). We found a slope for the L_X–L_B relationship steeper than previous investigations with *Einstein Observatory* data, with broad dispersion about the fit line. The observed L_X of the brightest galaxies were found to be comparable to either the energy released through supernovae or through gravitational infall. A correlation was confirmed between T_X and T_σ, using the 19 high-photon-count PSPC galaxies, with a slope steeper than that reported

by Davis & White (1996). We discussed a possible connection between the X-ray luminous galaxies and their gas temperatures with respect to T_σ, and suggested a possible connection between the observed X-ray luminosity and the environment in which each galaxy lies. Here, we present a more detailed analysis of the L_X–L_B correlation (§3.1), the relationship between T_X and T_σ (§3.2), and the role environment may play in the observed luminosities (§3.3).

3.1. The L_X–L_B Plane

There can be a large correction to the flux from 0.1–0.5 keV due to Galactic absorption, so we will limit our discussion to the luminosities determined for the 0.5–2.0 keV band (Table 3) which is fairly insensitive to Galactic absorption corrections. A logarithmic plot of L_B (derived from Faber et al. 1989 magnitudes) against L_X (Figure 2) for the sample is reproduced from Brown & Bregman (1998) with the addition of three dwarf galaxies: NGC 147, NGC 205, and NGC 221 (data processed according to the methods described in §2. The galaxy NGC 221 (M 32) is a detection of a single point source, with a calculated X-ray luminosity ($\log L_X = 37.39\,\mathrm{ergs\,s^{-1}}$) in good agreement with Burstein et al. (1997), while NGC 147 and NGC 205 are upper limits.

The X-ray-fainter galaxies appear to follow a linear relation (Figure 2) that can be compared to a stellar contribution derived from hard and soft X-ray components of Centaurus A ($\log\ L_X/L_B = 28.96\,\mathrm{ergs\,s^{-1}}/L_\odot$; Brown & Bregman 1998, and references therein). A stellar component may also be scaled from the M31 bulge, since it might be expected that the bulges of spiral galaxies exhibit the same spectral signatures as early-type galaxies dominated by stellar emission. The M31 contribution ($\log\ L_X/L_B = 29.21\,\mathrm{ergs\,s^{-1}}/L_\odot$ and $\log\ L_X = 38.93\,\mathrm{ergs\,s^{-1}}$, Irwin & Sarazin 1998) lies 0.3 dex higher than the Cen A stellar line, from which we infer that the stellar X-ray to optical luminosity ratio may not be a constant for all early-type systems.

The X-ray luminosities of the brightest galaxies in the sample can be compared to the maximum amount of energy produced by stellar motions and gravitational infall ($\log L_{grav} = 23.57 + (5/3)\log L_B$, Brown & Bregman 1998). This energy depends partly upon the shape of the potential well which is measured by the stellar velocity dispersion. The assumption is made that the thermalization of stellar mass loss is 100% efficient. Figure 2 also indicates that if the supernova rates of van den Bergh & Tammann (1991, upper line) are correct, supernovae can also provide energy sufficient to produced the high X-ray luminosities observed. The lower (by a factor of 4.7) supernova energy line ($\log L_{SN,2} = \log L_B + 30.22$) was determined using a supernova rate given by Turatto, Capellaro, & Benetti (1994) and

Table 3: X-Ray Galaxy Properties

	0.1–2.0 keV	0.5–2.0 keV	
Name	$\log L_X$ (erg s^{-1})	$\log L_X$ (erg s^{-1})	$\log \frac{L_X}{L_B}$ ($\frac{ergs^{-1}}{L_\odot}$)
N 0720	41.25 ±0.02	41.10 $^{+0.01}_{-0.02}$	30.15 ±0.06
N 1316	41.25 ±0.01	41.08 ±0.01	29.74 ±0.06
N 1344	39.75 $^{+0.14}_{-0.20}$	39.47 $^{+0.14}_{-0.20}$	28.81 $^{+0.15}_{-0.21}$
N 1395	41.20 ±0.02	41.04 ±0.02	30.02 ±0.06
N 1399	41.62 ±0.02	41.44 ±0.02	30.56 ±0.06
N 1404	41.40 ±0.02	41.27 ±0.02	30.53 ±0.06
N 1407	41.51 ±0.01	41.34 ±0.01	30.18 ±0.12
N 1549	40.47 $^{+0.03}_{-0.04}$	40.04 ±0.03	29.31 ±0.07
N 2768	40.57 ±0.06	40.41 ±0.06	29.62 ±0.13
N 3115	40.07 $^{+0.06}_{-0.07}$	39.74 $^{+0.06}_{-0.07}$	28.91 $^{+0.08}_{-0.09}$
N 3377	39.96 $^{+0.11}_{-0.15}$	39.42 $^{+0.11}_{-0.15}$	29.21 $^{+0.16}_{-0.19}$
N 3379	39.94 $^{+0.15}_{-0.22}$	39.78 $^{+0.15}_{-0.22}$	29.29 $^{+0.16}_{-0.23}$
N 3557	40.77 ±0.05	40.61 ±0.05	29.51 ±0.08
N 3585	39.97 $^{+0.09}_{-0.12}$	39.84 $^{+0.09}_{-0.12}$	29.12 $^{+0.11}_{-0.13}$
N 3607	40.97 ±0.02	40.82 ±0.02	29.64 ±0.12
N 3923	41.02 ±0.02	40.90 ±0.02	29.91 ±0.06
N 4125	41.24 ±0.03	41.01 ±0.03	29.85 ±0.12
N 4278	40.88 $^{+0.04}_{-0.05}$	40.55 $^{+0.04}_{-0.05}$	29.83 $^{+0.07}_{-0.08}$
N 4365	40.75 ±0.03	40.48 ±0.03	29.69 ±0.07
N 4374	41.25 ±0.02	41.09 ±0.02	30.10 ±0.06
N 4406	41.96 ±0.01	41.80 ±0.01	30.70 ±0.06
N 4472	41.93 ±0.00	41.77 ±0.00	30.45 ±0.06
N 4494	39.49 $^{+0.14}_{-0.22}$	39.28 $^{+0.14}_{-0.22}$	29.08 $^{+0.15}_{-0.23}$
N 4552	41.09 ±0.01	40.92 ±0.01	30.21 ±0.06
N 4621	39.91 $^{+0.08}_{-0.10}$	39.79 $^{+0.08}_{-0.10}$	29.01 $^{+0.14}_{-0.16}$
N 4636	41.95 ±0.01	41.81 ±0.01	30.85 ±0.06
N 4649	41.64 ±0.01	41.48 ±0.01	30.34 ±0.06
N 4697	40.41 ±0.02	40.13 ±0.02	29.55 ±0.06
N 5061	39.71 $^{+0.12}_{-0.16}$	39.54 $^{+0.12}_{-0.16}$	29.01 $^{+0.13}_{-0.17}$
N 5102	37.82 $^{+0.12}_{-0.17}$	37.70 $^{+0.12}_{-0.17}$	28.75 $^{+0.17}_{-0.21}$
N 5322	40.48 ±0.04	40.11 ±0.04	29.31 ±0.13
N 5846	42.15 ±0.01	42.01 ±0.01	30.75 ±0.12
I 1459	41.36 ±0.01	41.19 ±0.01	30.05 ±0.06
N 7507	40.25 $^{+0.19}_{-0.33}$	40.13 $^{+0.19}_{-0.33}$	29.31 $^{+0.20}_{-0.34}$

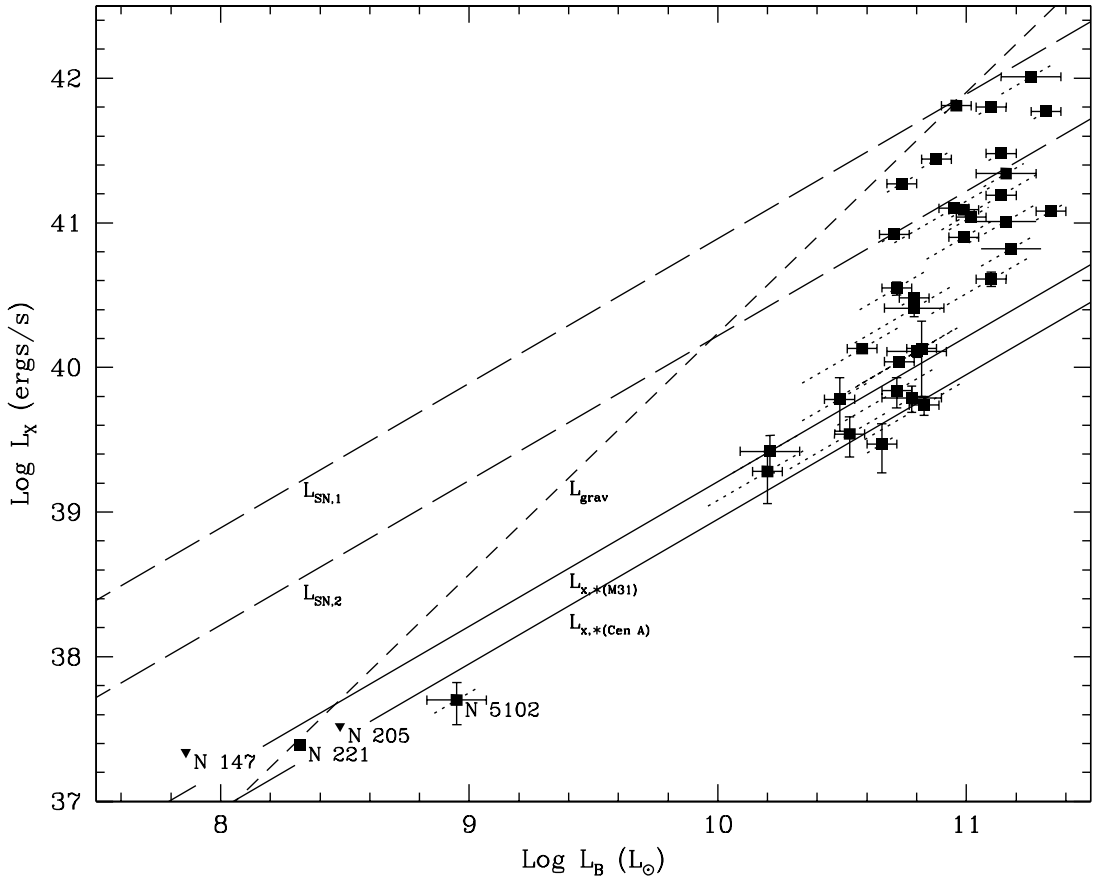

Fig. 2.— The optical blue luminosities (L_B) plotted against the $0.5 - 2.0$ keV X-ray luminosities (L_X) from the *ROSAT* PSPC and HRI instruments. In addition to our sample, the dwarf galaxies NGC 147, NGC 205, and NGC 221 are also shown. The uncertainties due to distances are shown as dashed lines of slope unity while errors due to distance-independent effects (e.g., photon statistics) are shown as the usual horizontal and vertical lines. The solid lines, $L_{X,*}$ are the stellar X-ray contributions as determined from M31 and the hard + soft components of Cen A, while the dashed lines labeled L_{SN} and L_{grav} represent the energy released from supernovae ($L_{SN,1}$ from van den Bergh & Tammann 1991, $L_{SN,2}$ from Turatto et al. 1994) or available from thermalization and gravitational infall.

assumes a SNe energy of 10^{51} ergs.

To determine the correlation between L_X and L_B, we implemented the ordinary least-squares (OLS) linear regression bisector method of Feigelson & Babu (1992) who discuss the applicability and effectiveness of several unweighted least-squares linear regression models to astronomical problems. The usual method employed by astronomers is the least squares Y-on-X (Y/X) fit, which minimizes residuals in Y. The OLS(Y/X) method is clearly preferred if it is known that one variable physically depends on another, or if the goal is to predict Y (L_X) given X (L_B). The goal of this study is not predicting L_X given L_B, but understanding the fundamental relationship between L_X and L_B. In this case, the assignment of a dependent or independent variable is uncertain, and so a symmetrical linear regression method is most appropriate as it is invariant to a change of variables (Isobe et al. 1990). Of the four OLS lines reviewed of this sort, the OLS bisector (the line bisecting the OLS(Y/X) and (X/Y) lines) is recommended.

The OLS bisector method yields a slope of 2.72±0.27 for our data (Table 4), which is slightly steeper than previously reported due to the application of a resampling procedure recommended for small samples (Feigelson & Babu 1992). In Table 4, we note that OLS(Y/X) fitting yields a flatter slope consistent with $m \approx 2.0$–2.3 (Eskridge et al. 1995, White & Davis 1997). There is an increase from 2.7 to 2.9 in the L_X–L_B slope if the background is chosen far from the galaxy center (see Table 4). The galaxy NGC 5102 is excluded from all fits primarily because of it's very low L_X/L_B ratio, which places it among the dwarf galaxies on the L_X–L_B plot (Figure 2). NGC 5102 has a very blue integrated color of $(B-V)^0_T = 0.58$ (de Vaucouleurs et al. 1976), and a low metallicity which suggests that this galaxy recently had a starburst episode, and its X-ray emission is consistent with that of stars (van Woerden et al. 1993).

An estimate of the hot gas contribution to the X-ray emission can be derived by subtracting a linear stellar component ($L_{X,*}$) from the data. The removal of the Cen A estimate of $L_{X,*}$ yields a slope of 3.32±0.46 (bisector, Table 4) for the L_X–L_B distribution. The bisector slope in this case was calculated using the methods of Isobe et al. (1990) since the distributed software of Feigelson & Babu (1992) does not accommodate upper limits. A gas component was not derived from M31 as we determined that the L_X magnitude of the M31 stellar component was greater than the lowest luminosity galaxies (NGC 1344, NGC 3115, and NGC 5102) at the 3σ level. Also, CO is abundant in the bulge of M31, which distinguishes it from early-type galaxies (Loinard, Allen, & Lequeux 1995), and it has been suggested that the M31 bulge represents a post-starburst stage (Rieke, Lebofsky, & Walker 1988).

Table 4: Least-Squares (OLS) Fits

	Bisector		Y/X	
	Intercept	Slope	Intercept	Slope
L_X-L_B, no stellar subtraction	11.06±2.92	2.72±0.27	16.57±2.49	2.22±0.23
L_X-L_B, no subtr.; alt. bkg. [a]	8.75±3.95	2.94±0.36	17.20±3.98	2.16±0.36
L_X-L_B, Cen A subtraction [b]	4.44±4.87	3.32±0.46	10.82±4.24	2.73±0.39
T_X-T_σ, B&B sample	0.26±0.14	1.43±0.34	0.04 ±0.13	0.90±0.34
T_X-T_σ, Davis & White	0.20±0.04	0.90±0.10	0.12 ±0.05	0.70±0.12

Fits performed in log-space, utilizing the bootstrap resampling procedure recommended for small samples. L_B in solar units. NGC 5102 not included in fits.
[a]Background taken far from galaxy center. Galaxies NGC 1344, NGC 3377, NGC 4494, NGC 5061, NGC 5102, & NGC 7507 not included.
[b]Hard plus soft X-ray components subtracted.

3.2. T_X–$T\sigma$ Correlation

Brown & Bregman (1998) confirm a correlation between the fitted X-ray gas temperature (T_X) and the stellar velocity dispersion temperature (T_σ), in addition to the L_X–L_B relationship. The slope of the logT_X–logT_σ relationship is found to be 1.43±0.34 (see Table 4), which is slightly steeper than a slope of unity that is expected in cooling flow models. Also not theoretically expected, is a large dispersion in T_X about the best fit line.

The slope to the temperature data differs from that reported by Davis & White (1996) who published temperatures for 30 galaxies. The causes of this difference are discussed briefly in Brown & Bregman (1998). One cause lies in the methods these two groups use in fitting the data. Our temperature data is reproduced in Figure 3a with the addition of a Y-on-X fitted line, and compared to the data of Davis & White (1996, Figure 3b) in illustration of the difference in statistical methods. For the Davis & White (1996) sample, we plot T_σ instead of σ, where T_σ is derived from Faber et al. (1989) and Dressler et al. (1991) velocity dispersions. As stated in §3.1, the regression method utilized is a function of the problem being addressed.

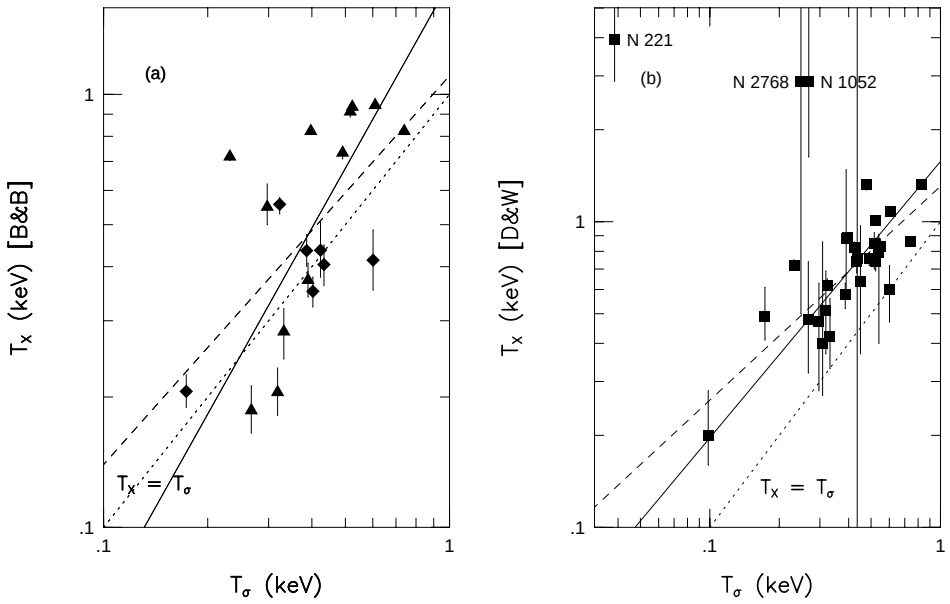

Fig. 3.— The stellar velocity dispersion temperature (T_σ) vs. the fitted gas temperature for nineteen galaxies in our sample (a), and the Davis & White sample (b). In both plots, the OLS bisector fit is represented by the solid line and the OLS(Y/X) fit is represented by the dashed line. The dotted line denotes the $T_X = T_\sigma$ relation. The errors in (a) are at the 90% confidence level.

Davis & White (1996) find gas temperatures everywhere hotter than the expected velocity dispersion temperature, which is a striking difference between their data and ours. Below $T_\sigma \approx 0.45$ keV we find a more or less symmetrical distribution of gas temperatures about the $T_X = T_\sigma$ line. In cases where we fit $T_X > 0.5$ keV, we find that our temperatures agree well with Davis & White (1996) for the same galaxies. Below $T_X = 0.5$ keV, our temperatures range from ∼25–60% below the values of Davis & White (1996). This difference cannot simply be the result of the number of temperature components allowed (see Brown & Bregman 1998), as three of our "low" T_X galaxies were fit with single-temperatures. Davis & White (1996) report extremely low solar abundances (Z $\leq$ 0.06 solar) for the three galaxies by allowing Z to be a fit parameter, and at low abundances, derived temperatures become higher.

A discussion of our data as compared to *ASCA* derived temperatures is given in Brown & Bregman (1998). Our temperatures are presented in Table 5 along with those of Davis & White (1996), and Buote & Fabian (1998) *ASCA* temperatures for comparison.

3.3. The galaxy environment

We suggested in our previous paper that the observed X-ray luminosity of a galaxy was strongly influenced by its environment because the most X-ray luminous galaxies were in clusters or in the centers of groups. Here, we examine this by quantifying the environment richness through the use of the local galaxy density, ρ. We determine which objects are X-ray luminous for their L_B by comparing L_X/L_B to the individual ρ of each galaxy in our sample.

In Figure 4, the ratio of the X-ray-to-optical luminosity is plotted against the Tully (1988) local density of galaxies (ρ) brighter than -16 mag in the vicinity of each sample galaxy. The galaxy density is calculated such that an isolated galaxy will have a local density of $\rho = 0.06$ galaxies Mpc^{-3} by virtue of its own presence. The local density in a richer environment, for example the center of the Virgo cluster, would be approximately 5 galaxies Mpc^{-3}. For our sample, no high luminosity systems are found in the most isolated environments ($\rho < 0.2$ galaxies Mpc^{-3}), where the median log L_X/L_B is plotted on Figure 4 at $\approx 29.1\,\mathrm{ergs\,s^{-1}}/L_\odot$. The upper and lower 25% quartile values for log L_X/L_B in this region are 29.2 and 28.8 respectively (both in $\mathrm{ergs\,s^{-1}}/L_\odot$). The highest luminosity galaxies are only found in the densest environments ($\rho > 0.79$ galaxies Mpc^{-3}), however lower luminosity ellipticals are also found in this region contributing to a collective median luminosity ratio of $\approx 30.2\,\mathrm{ergs\,s^{-1}}/L_\odot$, with log $L_X/L_B = 30.6\,\mathrm{ergs\,s^{-1}}/L_\odot$ at the upper 25% quartile and 29.7 $\mathrm{ergs\,s^{-1}}/L_\odot$ at the lower 25% quartile. For $0.2 < \rho < 0.8$ galaxies

Table 5: Gas Temperatures

Name	T_σ	T_X B&B	T_X D&W	T_X B&F	Name	T_σ	T_X B&B	T_X D&W	T_X B&F
N 0221	0.039	···	$3.94^{+1.73}_{-1.06}$	···	N 4261	0.549	···	$0.83^{+0.05}_{-0.06}$	···
N 0720	0.387	$0.436^{*}{}^{+0.039}_{-0.035}$	$0.58^{+0.05}_{-0.06}$	0.63	N 4278	0.450	···	$0.64^{+0.33}_{-0.27}$	···
N 1052	0.269	···	$2.88^{+5.92}_{-1.25}$	···	N 4365	0.390	···	$0.88^{+0.60}_{-0.29}$	···
N 1316	0.403	$0.351^{*}\pm0.028$	···	···	N 4374	0.524	···	0.74 ± 0.05	$0.70^{+0.05}_{-0.04}$
N 1344	0.163	···	···	···	N 4406	0.397	$0.823^{+0.010}_{-0.009}$	0.89 ± 0.01	$0.73^{+0.03}_{-0.02}$
N 1395	0.424	$0.437^{*}{}^{+0.071}_{-0.058}$	$0.82^{+0.04}_{-0.06}$	···	N 4472	0.524	$0.936^{+0.007}_{-0.006}$	1.01 ± 0.02	0.97
N 1399	0.610	0.944 ± 0.009	$1.08^{+0.02}_{-0.01}$	1.27	N 4486	0.831	···	$1.32^{+0.03}_{-0.04}$	···
N 1404	0.323	$0.557^{*}{}^{+0.021}_{-0.027}$	$0.62^{+0.03}_{-0.02}$	0.56	N 4494	0.300 [a]	···	$0.20^{+0.08}_{-0.04}$	···
N 1407	0.517	$0.913^{+0.027}_{-0.025}$	$0.85^{+0.07}_{-0.15}$	0.92	N 4552	0.434	$0.405^{*}{}^{+0.044}_{-0.042}$	$0.74^{+0.07}_{-0.06}$	···
N 1549	0.267	$0.186^{+0.026}_{-0.021}$	$0.48^{+0.26}_{-0.16}$	···	N 4621	0.367	···	···	···
N 2768	0.248	···	$2.87^{+16.13}_{-2.37}$	···	N 4636	0.232	0.717 ± 0.014	$0.72^{+0.03}_{-0.02}$	0.66
N 3115	0.450	···	···	···	N 4649	0.740	0.823 ± 0.015	$0.86^{+0.02}_{-0.01}$	0.83
N 3377	0.108	···	···	···	N 4696	0.478 [b]	···	$1.32^{+0.04}_{-0.05}$	···
N 3379	0.257	···	···	···	N 4697	0.173	$0.206^{*}{}^{+0.019}_{-0.017}$	$0.49^{+0.12}_{-0.08}$	···
N 3557	0.541	···	$0.79^{+0.12}_{-0.39}$	···	N 5061	0.233	···	···	···
N 3585	0.308	···	$0.40^{+0.46}_{-0.13}$	···	N 5102	0.500 [a]	···	···	···
N 3607	0.390	$0.372^{+0.035}_{-0.032}$	···	···	N 5322	0.319	$0.205^{+0.028}_{-0.024}$	$0.51^{+0.18}_{-0.14}$	···
N 3923	0.297	$0.549^{+0.071}_{-0.049}$	$0.47^{+0.16}_{-0.19}$	0.64	N 5846	0.491	$0.733^{+0.024}_{-0.023}$	$0.76^{+0.03}_{-0.04}$	$0.67^{+0.04}_{-0.03}$
N 4105	0.436 [b]	···	$0.76^{+4.40}_{-0.69}$	···	I 1459	0.602	$0.414^{*}{}^{+0.072}_{-0.061}$	$0.60^{+0.12}_{-0.13}$	2.69
N 4125	0.332	$0.283^{+0.037}_{-0.038}$	$0.42^{+0.14}_{-0.09}$	···	N 7507	0.361	···	···	···

B&B - Brown & Bregman (1998). D&W - Davis & White (1996). B&F - Buote & Fabian (1998). Only B&F galaxies concurrent with B&B listed. All temperatures given in keV. T_σ derived from Faber et al. (1989) values. $H_0 = 50$ km/s/Mpc used throughout. Starred values in the T_X B&B column denote a two temperature fit value where the 2nd component is fixed at 2.0 keV. B&B errors at the 90% confidence level.

[a] Adopted value for T_σ.

[b] T_σ from Dressler et al. (1991).

Mpc^{-3}, the median luminosity ratio has a moderate value of $\log(L_X/L_B) \approx 29.6\,\mathrm{ergs\,s^{-1}}/L_\odot$ and upper and lower 25% quartile log L_X/L_B values of 29.3 and 30.0 respectively (in $\mathrm{ergs\,s^{-1}}/L_\odot$).

The data appear to follow a correlation albeit with broad dispersion, and there is a lower limit to the luminosity ratio for $-1.2 < \log \rho < 0.6$, with no galaxies found below log $L_X/L_B = 28.8\,\mathrm{ergs\,s^{-1}}/L_\odot$. We applied statistical tests to the data to quantify the apparent correlation. Three non-parametric tests for bivariate data, Kendall's Tau, Spearman's Rho, and Cox Proportional Hazard, were performed, each of which determined a correlation in the data at better than the 99.7% confidence level.

We additionally examined the L_X residuals for the OLS(Y/X) fit, excluding NGC 5102, as they might relate to the galaxy environment (see Figure 5). The residuals are defined to be the difference between L_X and the OLS bisector fit to L_X and L_B. The Kendall's Tau test indicates a correlation exists at $> 99\%$ confidence. The correlation implies that the galaxies brightest for their optical luminosity (i.e, NGC 1399, NGC 4636, NGC 4552) are found in the spatially densest regions (relative to the rest of the sample). Occasionally, a galaxy with a low L_X, given L_B, is found in a dense environment indicating that complex mechanisms affect observed X-ray luminosities.

The fitted X-ray temperatures, as a function of spatial density, exhibit a weak correlation at the 92-95% confidence level, depending upon if one uses the Kendall's Tau test, the Spearman's Rho test, or the Cox Proportional Hazard model (Figure 6a). The hottest galaxies ($kT_X \sim 0.8$ keV) are found in a range of environments as are galaxies with $kT_X \sim 0.45$ keV. The ratio of T_X to T_σ as a function of density exhibits an even weaker correlation, as shown in Figure 6b.

3.4. Malmquist bias

The issue of bias is an important one for our sample, so we have addressed the statistical and geometrical effects that are often discussed as Malmquist bias. One effect is of concern whenever measured distances contain uncertainty. Along a line of sight, as one goes farther in distance, the volume of space associated with a given solid angle increases. This has the effect of giving greater weight to larger distances. This is the "classical" Malmquist bias, and is corrected for in the distance measurements used in our analyses (Faber et al. 1989).

The other type of Malmquist bias occurs in magnitude-limited samples and reflects the fact that the intrinsic luminosity function is not being equally or completely sampled at all

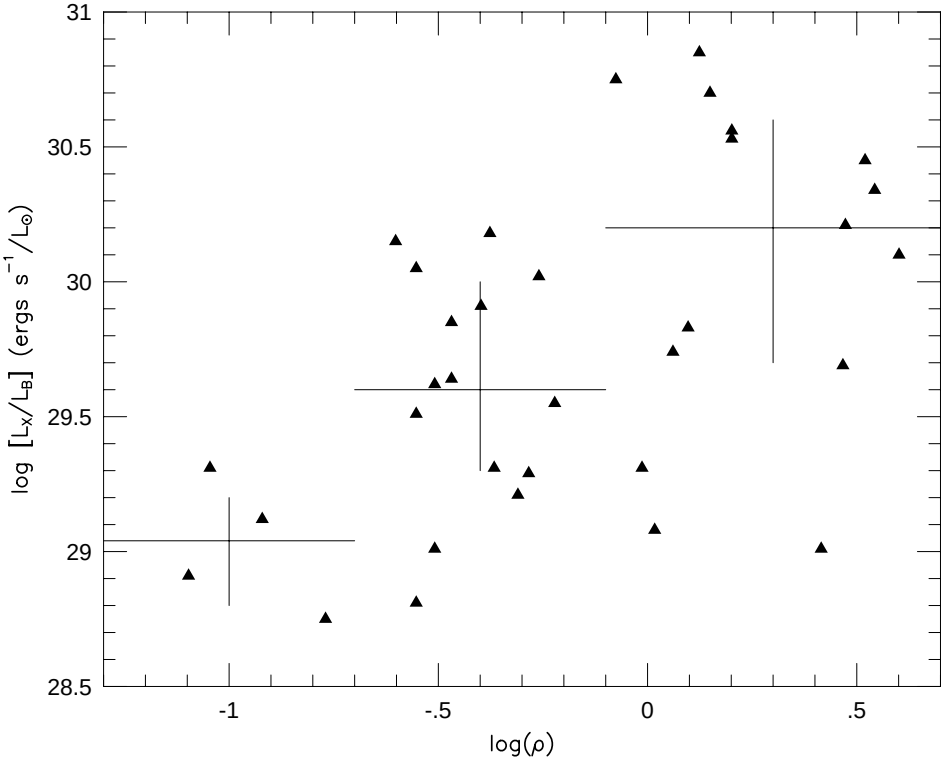

Fig. 4.— The luminosity ratio (L_X/L_B) vs. the local density of galaxies brighter than -16 mag in the vicinity of each galaxy (Tully 1988 values). The horizontal lines delineate the width of each bin and mark the median ration within each bin. The vertical lines are the magnitude of the upper and lower quartile values within each bin.

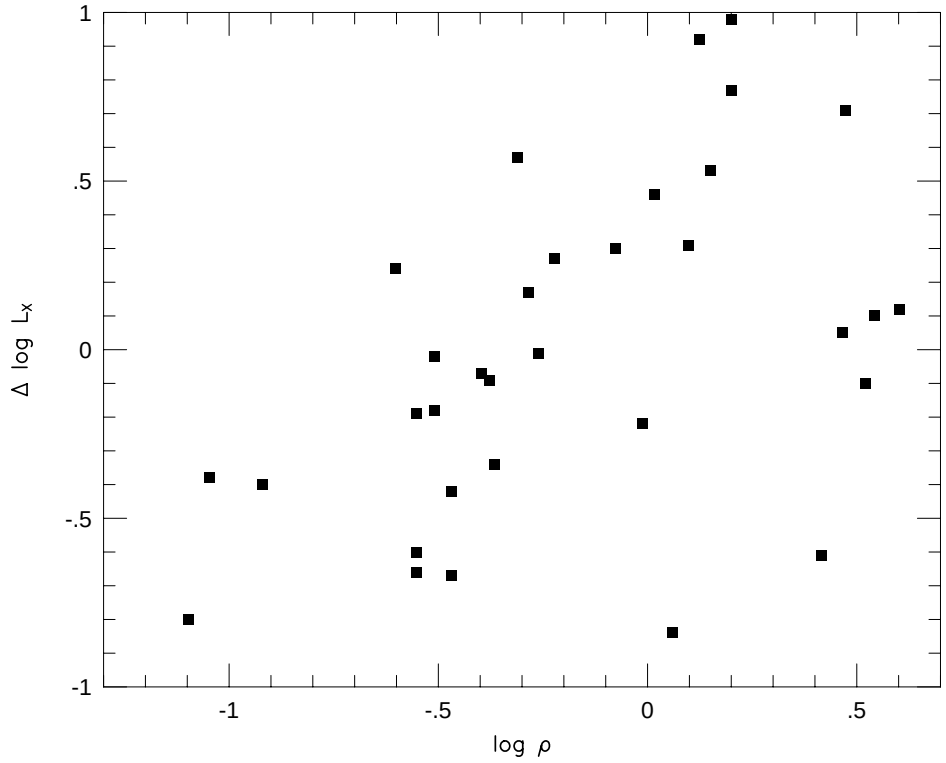

Fig. 5.— The residuals in L_X vs. the local density of galaxies brighter than -16 mag in the vicinity of each galaxy (Tully 1988 values). The residuals in L_X are relative to the least squares fit between L_X and L_B. Error bars have been repressed in this plot.

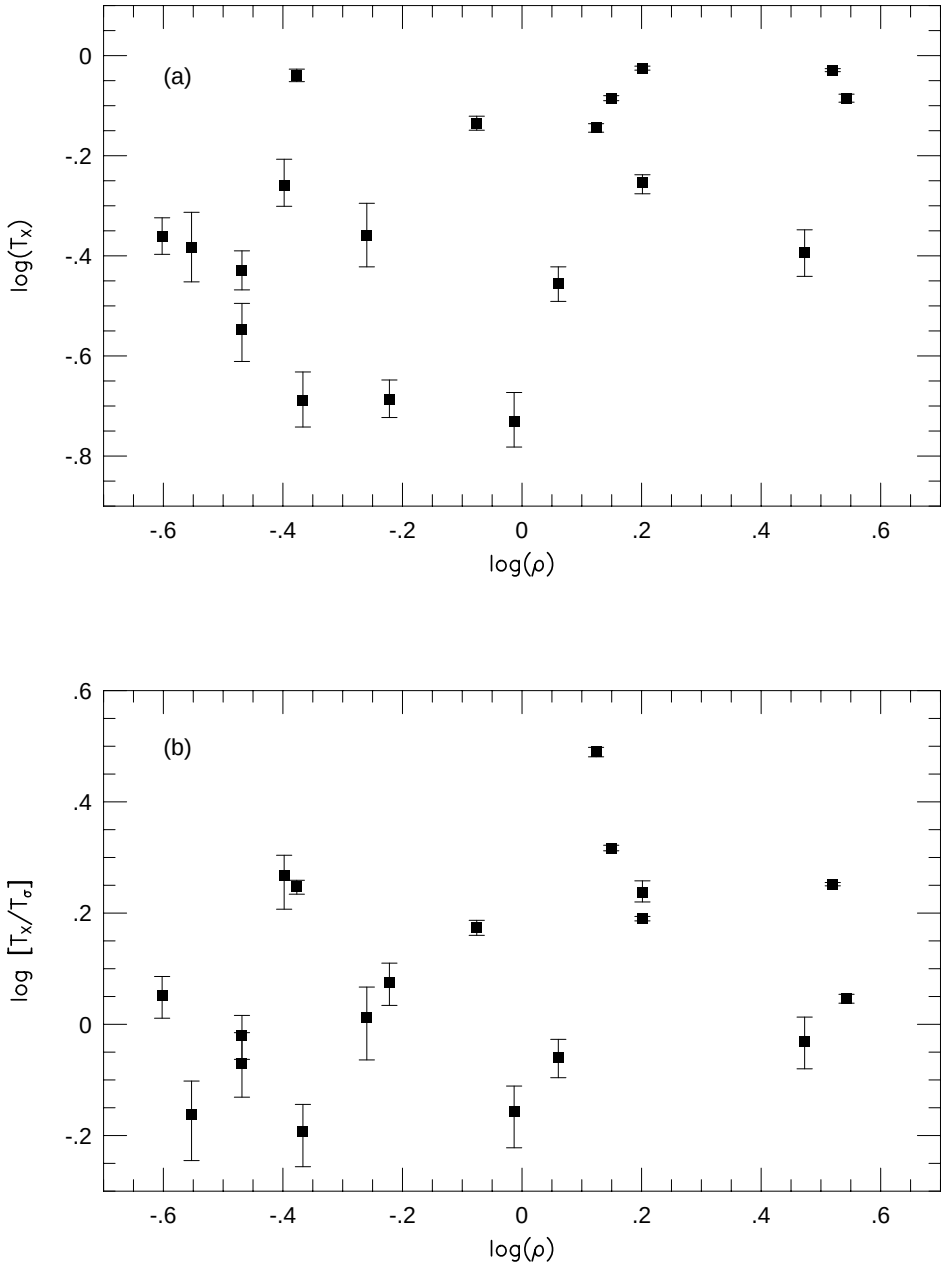

Fig. 6.— The gas temperature (T_X) vs. the local density of galaxies brighter than -16 mag in the vicinity of each galaxy (Tully 1988 values, 6a), and the temperature ratio (T_X/T_σ vs. ρ, 6b). The errors in T_X are at the 90% confidence level.

distances. For the most distant galaxies, only the high luminosity part of the luminosity function is sampled, whereas for the nearest galaxies, much more of the luminosity function is sampled. Although this is an important issue for some investigations, such as those using standard candles as distance indicators (e.g., Teerikorpi 1997), it is not important for this study, which does not require that the Schecter luminosity function be fully sampled. Our sample merely requires that the galaxies be representative of those that comprise the Schecter luminosity function, and that they were chosen in a fashion that does not bias the X-ray luminosity. These galaxies where chosen independently of their X-ray properties, each was detected in X-rays, and they lie far above the magnitude limit of the Faber et al. (1989) sample, so this should comprise an unbiased sample.

4. Discussion and Conclusions

4.1. The Role of Environment

One of results of our work is the demonstration that environment has a central influence on the X-ray luminosity as seen in the positive correlation of the L_X/L_B ratio with galaxy density. In the lowest density environments, only X-ray faint galaxies are found (low L_X/L_B ratios), and the galaxies with the highest L_X/L_B ratios are found in fairly dense environments. However, galaxies in dense environments exhibit a wide range in L_X/L_B, suggesting that environment does not have the same effect on all galaxies, and we suggest a natural explanation for this.

The distribution of L_X/L_B in Figure 4 reveals that there is a positive correlation between local environmental richness and X-ray brightness, but with significant dispersion at moderate and high galaxy density. In an effort to understand this distribution, it is important to recognize that environment can have both positive and negative effects on the X-ray brightness of a galaxy (e.g., Takeda, Nulsen, & Fabian 1984). Groups and clusters with a significant ambient medium can lead to stripping of the interstellar gas from a galaxy, leading to a substantial reduction in L_X/L_B. However, for galaxies moving slowly through relatively cool clusters or groups, the galaxy may be able to accrete this external material, increasing L_X/L_B (Brighenti & Mathews 1998). Also, an ambient group or cluster medium could stifle galactic winds, should they exist, causing the galaxy to retain its hot gas locally, which also will increase L_X/L_B. Therefore, galaxies in clusters or groups would have a range of L_X/L_B, where the low values are determined by galaxies where stripping or winds occur, and the high values represent systems that are accreting the ambient material or having their winds stifled. In very rich clusters, like Coma, stripping is probably the dominant process, but none of the galaxies in our sample lie in such a rich system. The

richest cluster in this sample is Virgo, where stripping is expected to occur in some of the galaxies, but not most of them (Gaetz, Salpeter, & Shaviv 1987).

The role of environment has been previously examined by White & Sarazin (1991) using *Einstein Observatory* data to determine if a correlation exists between local galaxy density and L_X. White & Sarazin (1991) find the number of bright, neighboring galaxies within various projected distances from each X-ray galaxy, and perform linear regressions of log L_X against log L_B and the local density of galaxies. They conclude that the large dispersion in L_X is not significantly reduced by taking into account the individual local galaxy density, which may be due to uncertainties in the numbers of neighbors found. White & Sarazin (1991) then binned the X-ray sample in order to reduce statistical error. The X-ray sample is divided into four subsets: high-L_X ($\log L_X/L_B \gtrsim 30\,\mathrm{ergs\,s^{-1}}/L_\odot$) detections, high-$L_X$ upper limits, low-L_X detections, and low-L_X upper limits. The total number of bright galaxies (again, within various projected distances) around all galaxies in each subset is calculated yielding an averaged number of bright galaxies per X-ray galaxy for each subgroup. They find that low-L_X galaxies have $\sim 50\%$ more neighbors than high-L_X galaxies, which the authors argue is expected if ram-pressure stripping is a major factor in the L_X dispersion.

The method of White & Sarazin (1991) is significantly different from ours. Whereas they bin an incomplete sample of *Einstein Observatory* data and look at bright neighbors in various projected distances, we use the tabulated local galaxy density data of Tully (1988) for each galaxy in our complete sample. The Tully local density is calculated using a three-dimensional grid spaced at 0.5 Mpc. Also, our data includes X-ray fainter galaxies, which allows us to extend the range of X-ray-to-optical luminosity ratios. Our data extends down to $\log L_X/L_B = 28.8\,\mathrm{ergs\,s^{-1}}/L_\odot$ versus the Canizares, Fabbiano, & Trinchieri (1987; used by White & Sarazin 1991) data which extends down to $\log L_X/L_B = 29.2\,\mathrm{ergs\,s^{-1}}/L_\odot$. Since none of the galaxies in these samples lie in rich environments (i.e., > 4 galaxies per Mpc^3), we cannot determine if ram-pressure stripping effects becomes significant in the observed X-ray luminosity in very dense environments.

4.2. The Importance of Galactic Winds

The extremely low values of L_X/L_B seen in isolated galaxies is probably the strongest evidence in favor of galactic winds. The X-ray emission from these systems is so low that one is probably detecting the X-ray contribution from stars rather than gas, indicating that these galaxies are not gas-rich. For these galaxies, an ambient group or cluster medium is not detected and they do not lie in a high velocity dispersion group, so stripping is unlikely

to occur. Furthermore, the rate of supernova energy input is probably adequate to drive a galactic wind, as discussed below. Therefore, the most viable mechanism for rendering the galaxies X-ray weak is through galactic winds (see Pellegrini & Ciotti 1998, and references therein).

Galactic winds will occur if the supernova heating rate is sufficient to raise the temperature of the mass loss from stars above the escape temperature (from the galaxy center). A steady-state galactic wind will obey Bernoulli's law, which for a flow that has a small flow velocity when it reaches large radius is $\frac{5P}{2\rho} + \Phi = 0$, where Φ is the gravitational potential and $\frac{5P}{2\rho}$ is the enthalpy. For a steady-state wind from the center of a galaxy where $\Phi(0) = 8\sigma^2$,

$$T_{wind} = \frac{16}{5}\sigma^2 \mu m_p/k \tag{3}$$

The variable μ is the mean molecular weight, m_p is the proton mass, and k is the Boltzmann constant. We use the supernova rate of Cappellaro et al. (1997), and energy per supernova of 10^{51} ergs, and the stellar mass loss rate of Faber & Gallagher (1976) to determine gas temperature entering the system:

$$T_{gas} = (\alpha_{SN} T_{SN} + \alpha_* T_*)/(\alpha_{SN} + \alpha_*) \tag{4}$$

where α_* and α_{SN} are the mass loss rates from stars and supernovae (see, e.g., Mathews & Brighenti 1997).

We then find that the most optically luminous galaxy that can sustain a total wind occurs at $L_B = 5 \times 10^{10} L_\odot$. Less luminous galaxies can drive a wind, provided that high ambient pressure from the surrounding environment does not prevent it. For galaxies more luminous than about $1.5 \times 10^{11} L_\odot$, the radius beyond which a wind can exist is far enough out that most of the stellar mass loss is retained by the galaxy (for galaxies with more complex models, partial winds may be more common; see Pelligrini & Ciotti 1998). The largest uncertainty in estimating these values for L_B is the energy released per supernova, which may be uncertain by about a factor of two.

Previously, we offered the suggestion that the galaxies with high L_X/L_B values were X-ray bright because galactic winds were stifled (contained) by a high-pressure ambient medium. This is energetically possible if the supernova rate is correctly given by van den Bergh & Tammann (1991), whose rate differs by about a factor of three from Cappellaro et al. (1997; see Figure 2). The primary discrepancy between the two rate calculations is the correction for the inability to detect supernovae against the ambient light of the galaxy. A correction by a factor of three was suggested by van den Bergh & Tammann (1991), while Cappellaro et al. (1997) argue that the correction factor is only about 40%. We calculated the distance from the center of an elliptical galaxy within which a point source near the

magnitude limit of these surveys would fall below the 5σ detection threshold, for a typical elliptical galaxy in these surveys. We find that only 5-30% of the supernovae would have been missed due to this effect, similar to the more accurate calculation of Cappellaro et al. (1997).

The supernova heating rate of Turatto, Capellaro, & Benetti (1994; line $L_{SN,2}$ in Figure 2) is insufficient to account for the X-ray emission from the highest L_X/L_B systems, which are up to a factor of three above this line (an energy of 10^{51} erg per supernova is used). Unless the energy per supernova has been underestimated by a factor of three, we consider unlikely our original suggestion that stifled winds can explain the highest L_X/L_B systems. The source of energy in these high luminosity systems is most likely gravitational, supplied by accretion onto the system, as discussed by Mathews & Brighenti (1998) and Brighenti & Mathews (1999). They show that the temperature and density distributions of hot gas in X-ray luminous galaxies, such as NGC 4472, are consistent with their calculations.

4.3. An Overall Explanation of the L_X–L_B Distribution

Previously, there was hope that the cooling flow model could provide a satisfactory explanation for the observed $\log L_X$–$\log L_B$ distribution. An L_X–L_B correlation with a slope of about 1.7 was predicted, which was similar to observations, and the dispersion about this correlation was treated as perturbations due (in part) to differences in galaxy evolution. The picture that we present is fundamentally different. We suggest that the steep observed correlation is due to the transition from galaxies with total winds, to those with partial winds, to those where the gas is retained and can accrete additional material. As calculated above, we expect this transition from winds to retained gas to occur in the range $10.7 < \log L_B(L_\odot) < 11.2$. Below $\log L_B = 10.7(L_\odot)$, one only finds galaxies with small values of L_X/L_B, as would be expected for systems with total winds. Also, all galaxies with $\log L_B > 11.2$ have L_X/L_B values well above that for purely stellar emission, consistent with retaining their gas. Of equal importance is the influence of environment, which can remove galactic gas through stripping, but can also help galaxies retain their gas by stifling winds, and can add to the galactic gas content through accretion.

A critical difference between our picture and most others is that heating by supernovae can be comparable to, if not greater than the heating by the thermalization of stellar ejecta. This suggestion is not in complete agreement with other models or with some observations, the disagreement centering around the importance of winds and the metal enrichment introduced by the supernovae. Brighenti & Mathews (1999) study massive galaxies and use a supernova rate that is less than half the value determined by Cappellaro et al.

(1997). With these supernova rates and galactic potential wells, winds are not important. They show that a range of nearly an order of magnitude in L_X/L_B can be introduced by truncation of the galaxy as it interacts with neighbors (Brighenti & Mathews 1999).

However, the observed range in L_X/L_B is two orders of magnitude, and when the stellar contribution is removed, the range in L_X/L_B due to the gas alone substantially exceeds two orders of magnitude. It is unlikely that truncation alone will produce the wide range in L_X/L_B. Also, in their model, one might expect that truncation would be least important in regions of low galaxy density, leading to high values of L_X/L_B in such regions. In conflict with this expectation, we find that galaxies in the lowest density environments only have low values of L_X/L_B. The great range of L_X/L_B and the finding that fairly isolated galaxies have low values of L_X/L_B is consistent with expectations of a model that incorporates galactic winds.

A discussion of supernova rates also introduces an apparent conflict between the expected and observed metallicity of the X-ray emitting gas (see Brown & Bregman 1998). For the standard cooling flow picture and the rates given by Cappellaro et al. (1997), the metallicity should be several times solar instead of near-solar (Loewenstein & Mushotzky 1997; Buote 1999). However, the metallicities are measured only for the most luminous galaxies, and these are precisely the ones for which accretion of circumgalactic gas dominates the gas content. The metallicity prediction must be revised downward due to the diluting effects of the accreted gas, which may reduce the metallicity into the observed range.

4.4. Predictions of the Models

The various suggestions made by us and others has several immediate predictions that will be tested by upcoming observations. First, the amount of the stellar contribution to the X-ray emission should be spatially resolved by *Chandra*, leading to a clear determination of this value, and probably a determination of the spectrum, separated from the spectrum of the hot gas. Another important test will be the measurement of the rate of cooling gas, since it should be low if supernovae cause galactic winds and approximately the stellar mass loss rate if cooling flows are uniformly present. We predict that the low L_X/L_B galaxies will show little evidence of cooling gas, which will be measured through the O VIII and O VII X-ray lines with *Chandra*, and through the O VI line with *FUSE*. The high L_X/L_B galaxies should have cooling rates similar to the stellar mass loss rate, if not greater, although most models agree on this prediction. Cooling flow models should show a significant metallicity gradient from the outer to the inner parts, reflecting the stellar metallicity gradient, and

this effect should be even more pronounced for galaxies that are accreting material from the surrounding group or cluster. Finally, the ongoing optical supernova searches, being carried out with modern CCD techniques, should yield an improved determination of the supernova rate.

We would like to thank a variety of people for valuable discussion: J. Irwin, J. Mohr, P. Hanlan, R. White, M. Loewenstein, G. Worthey, J. Parriott, M. Roberts, D. Hogg, and R. Mushotzky. Special thanks is due to the members of the *ROSAT* team and to the archiving efforts associated with the mission. Also, we wish to acknowledge the use of the NASA Extragalactic Database (NED), operated by IPAC under contract with NASA; SLOPES, which implements the methods presented in Isobe et al. (1990), Babu & Feigelson (1992), and Feigelson & Babu (1992); ASURV (Isobe & Feigelson 1990), which implements the methods presented in Isobe, Feigelson, & Nelson (1986). NASA has provided support for this work through grants NAGW-2135, NAG5-1955, and NAG5-3247; BAB would like to acknowledge support through a NASA Graduate Student Researchers Program grant NGT-51408, and the support of the National Academy of Sciences postdoctoral associate program.

REFERENCES

Babu, G. J., & Feigelson, E. D. 1992, Communications in Statistics, Simulation & Computation, 21, 533

Bauer, F., & Bregman, J. N. 1996, ApJ, 457, 382

Brighenti, F., & Mathews, W. G. 1998, ApJ, 495, 239

Brighenti, F., & Mathews, W. G. 1999, ApJ, 512, 65

Brown, B. A., & Bregman, J. N. 1998, ApJ, 495, L75, astro-ph/9712209

Buote, D. A. 1999, MNRAS, in press, astro-ph/9903278

Buote, D. A., & Fabian, A. C. 1998, MNRAS, 296, 977

Burstein, D., Jones, C., Forman, W., Marston, A. P., & Marzke, R. O. 1997, ApJS, 111, 163

Canizares, C. R., Fabbiano, G., & Trinchieri, G. 1987, ApJ, 312, 503

Cappellaro, E., Turatto, M., Tsvetkov, D.Y., Bartunov, O.S., Pollas, C., Evans, R., & Hamuy, M. 1997, A&A, 322, 431

David, L. P., Forman, W., & Jones, C. 1991, ApJ, 369 121

Davis, D. S., & White, R. E. 1996, ApJ, 470, L35

D'Ercole, A., Renzini, A., Ciotti, L., & Pellegrini, S. 1989, ApJ, 341, L9

Donnelly, R. H., Faber, S. M. & O'Connell, R. M. 1990, ApJ, 354, 52

Dressler, A., Faber, S. M., & Burstein, D. 1991, ApJ, 368, 54

Eskridge, P. B., Fabbiano, G., & Kim, D.-W. 1995, ApJS, 97, 141

Fabbiano, G. 1989, ARA&A, 27, 87

Faber, S. M., & Gallagher, J. S. 1976, ApJ, 204, 365

Faber, S. M., Wegner, G., Burstein, D., Davies, R. L., Dressler, A., Lynden-Bell, D., & Terlevich, R. J. 1989, ApJS, 69, 763

Feigelson, E. D., & Babu, G. J. 1992, ApJ, 397, 55

Gaetz, T. J., Salpeter, E. E., & Shaviv, G. 1987, ApJ, 316, 530

Irwin, J. A., & Sarazin, C. L. 1998, ApJ, 494, 33

Isobe, T., & Feigelson, E. D. 1990, BAAS, 22, 917

Isobe, T., Feigelson, E. D., & Nelson, P. I. 1986, ApJ, 306, 490

Isobe, T., Feigelson, E. D., Akritas, M. G., & Babu, G. J. 1990, ApJ, 364, 104

Loewenstein, M., & Mathews, W. G. 1987, ApJ, 319, 614

Loewenstein, M., & Mathews, W. G. 1991, ApJ, 373, 445

Loewenstein, M., & Mushotzky, R. F. 1997, Proceedings of IAU Symposium 187 on Cosmic Chemical Evolution

Loinard, L., Allen, R. J., & Lequeux, J. 1995, A&A, 301, 68

Mathews, W. G., & Brighenti, F. 1997, ApJ, 488, 595

Mathews, W. G., & Brighenti, F. 1998, ApJ, 503, 15

McMillan, R., Ciardullo, R., & Jacoby, G. H. 1994, AJ, 108, 1610

Pellegrini, S. & Ciotti, L. 1998, A&A, 333, 433

Rieke, G. H., Lebofsky, M. J., & Walker, C. E. 1988, ApJ, 325, 679

Takeda, H., Nulsen, P. E. J., & Fabian, A. C. 1984, MNRAS, 208, 261

Teerikorpi, P. 1997, ARA&A, 35, 101

Tully, R. B. 1988, Nearby Galaxies Catalog (Cambridge University: Cambridge)

Turatto, M., Cappellaro, E., & Benetti, S. 1994, AJ, 108, 202

van den Bergh, S., & Tammann, G. A. 1991, ARA&A, 29, 363

van Woerden, H., van Driel, W., Braun, R., & Rots, A. H. 1993 A&A, 269, 15

de Vaucouleurs, G., de Vaucouleurs, A., and Corwin, H. G. 1976, *Second Reference Catalogue of Bright Galaxies* (RC2), (Austin: Univ. of Texas Press)

Vedder, P. W., Trester, J. J., & Canizares, C. R. 1988, ApJ, 332, 725

White, R. E. III, & Davis, D. S. 1997, in Galactic and Cluster Cooling Flows, ed. N. Soker (ASP: San Francisco), p. 217

White, R. E. III, & Sarazin, C. L. 1991, ApJ, 367, 476